Handover Skipping for LiFi

Handover Skipping for LiFi

Xiping Wu and Harald Haas

LiFi Research and Development Centre

Institute for Digital Communications

School of Engineering, The University of Edinburgh

EH9 3JL, Edinburgh, UK

{xiping.wu, h.haas}@ed.ac.uk

Abstract

This work studies handover skipping, which is able to transfer the user between two non-adjacent access points (APs), in light fidelity (LiFi) networks. LiFi is an emerging wireless communication technology, which operates in a way similar to wireless fidelity (WiFi) but uses light waves as a medium. Compared to WiFi, LiFi has a relatively shorter range and the coverage range of a single AP is limited. This could cause more frequent handovers and thus handover skipping techniques are required. The conventional handover skipping methods rely on the information on the user's trajectory, which is not ready to use at the AP. Based on reference signal received power (RSRP), a novel handover skipping method is proposed in this paper. The new method combines the value of RSRP and the change in RSRP to determine the handover target. Since RSRP is already used in the current handover schemes, the proposed method does not require additional feedback. Results show that compared to the standard handover scheme and the conventional handover skipping method, the proposed method can reduce handover rate by up to 29% and 17%, and improve throughput by up to 66% and 26%.

Index Terms

[1]This paper was presented in part at IEEE VTC Spring 2019 [1].

Light fidelity (LiFi), handover skipping, reference signal received power (RSRP), user mobility

I. INTRODUCTION

Global mobile data traffic will increase sevenfold between 2017 and 2022, reaching 77.5 exabytes per month by 2022, and traffic from wireless fidelity (WiFi) and mobile devices will account for 71 percent [2]. Globally, there will be nearly 549 million public WiFi hotspots by 2022, up from 124 million hotspots in 2017 [2]. The high-density WiFi deployment would cause sever signal interference due to the limited spectrum resource of radio frequency (RF). To tackle the looming spectrum shortage in RF, wireless communication technologies based on extremely high frequencies have attracted significant attentions, such as millimetre wave (mmWave) communications [3], massive multiple-input multiple-output (MIMO) [4], and visible light communications (VLC) [5]. The wireless networking use case of VLC is termed light-fidelity (LiFi) [6], which operates in a way similar to WiFi but uses light waves as a signal bearer. Unlike RF communications, the LiFi access points (APs) can be integrated in the existing light infrastructure, e.g. light-emitting diode (LED) lamps, realising a dual purpose system offering illumination and communication. Recent research shows that with a single off-the-shelf LED, LiFi is capable of achieving peak data rates above 10 Gbps [7]. Also, LiFi offers many other advantages over WiFi, including: i) a vast and licence-free spectrum; ii) secure communication as light does not penetrate opaque structures; and iii) the availability in RF-restricted areas such as underwater and hospitals [8].

Due to inherently high propagation losses, all wireless communication technologies based on extremely high frequencies, including LiFi, have a relatively short range. Specifically, the LiFi AP has a coverage area of approximately 2-3m in diameter [9]. This enables LiFi to achieve a very high area spectral efficiency through frequency reuse [10]. However, in such an ultra-dense network, the handover process becomes challenging mainly due to two issues: i) readily occurring ping-pong effects and ii) relatively short cell dwell time (CDT). The signal strength

strategy (SSS) method, which always connects the user to the AP that provides the highest reference signal received power (RSRP), thus becomes hugely suboptimal for LiFi. In order to suppress the ping-pong effect, the standard handover scheme in long term evolution (LTE) [11] uses the idea of hysteresis, which prolongs the handover decision for an amount of time. However, this handover scheme is not capable of tackling the second issue.

In order to avoid the frequent handovers in ultra-dense networks, the concept of handover skipping is introduced [12]–[14]. A topology-aware skipping scheme is proposed in [12], which sets a pre-defined threshold with respect to the chord length of the cell. A similar method is reported in [13], but extended to multiple AP association. The authors in [14] develop a velocity-aware handover approach, which performs different skipping strategies according to the user's velocity, including: best connected strategy, femto skipping strategy, femto disregard stratey and macro skipping strategy. However, the above methods are all based on the knowledge of the user's trajectory. As a result, they have the following limitations: i) the measurement of the user's trajectory is less accurate in an indoor scenario due to uncontrollable errors caused by the multiple reflections at surfaces; and ii) extra feedback is required to send this information to the APs. To the best of the authors' acknowledge, no handover skipping method that does not rely on the user's trajectory has so far been proposed.

In this paper, an RSRP-based handover skipping method is proposed. The new method exploits the change in RSRP to reflect whether the user is moving towards the central area of an AP. Through a weighted average of the value of RSRP and the change in RSRP, the novel method is able to determine whether to skip a certain AP. As the change in RSRP is related to the user' velocity, the proposed method is velocity-aware. Unlike the trajectory-based methods, the proposed method does not need extra feedback since RSRP is already used in the standard handover scheme. Therefore, the proposed method can be readily implemented in practice. Also, the performance of the proposed method in terms of handover rate and coverage probability is analysed. Furthermore, the optimal weight coefficient is studied. Simulation results show that

against the standard handover scheme, the proposed method can greatly reduce the handover rate and improve the throughput.

The remainder of this paper is organised as follows. In Section II, the system model of an indoor LiFi network and the channel model are described. Section III introduces the standard handover scheme in LTE. The novel handover skipping method is proposed in Section IV. In Section V, the handover rate and coverage probability of the proposed method are theoretically analysed. Simulation results are presented in Section VI. Finally, conclusions are drawn in Section VII.

II. System Model

Consider an indoor wireless network consisting of a number of LiFi APs. The system is considered to be time division duplex, and we focus on downlink communications. Each LiFi AP is built in a ceiling LED lamp, facing downwards perpendicularly. The LiFi APs use different spectra and therefore do not interfere with each other. A single photodiode (PD) pointing upwards perpendicularly is fitted at the user. Though the issue of random receiving orientaions has been identified [15], the PD can keep facing upwards by using a rotation device to compensate the change in orientation. The user is assumed to move around in the room, following the random waypoint (RWP) model [16].

A LiFi channel is comprised of two components: line-of-sight (LoS) and non line-of-sight (NLoS) paths. Here only first-order reflections are considered since second-order reflections typically contribute little [17]. Fig. 1 illustrates the LoS and first-order NLoS paths of a LiFi channel. Let i and u denote the AP and the user, respectively. The LoS path corresponds to the straight-line distance between the AP and the user, which is denoted by $d_{i,u}$. Let $\phi_{i,u}$ and $\psi_{i,u}$ respectively denote the angles of irradiance and incidence. The channel gain of LoS is denoted by $H_{\text{LoS}}^{i,u}$, and it is given by [17, eq. (10)]:

$$H_{\text{LoS}}^{i,u} = \frac{(m+1)A_{\text{pd}}}{2\pi d_{i,u}^2} \cos^m(\phi_{i,u}) g_f g_c(\psi_{i,u}) \cos(\psi_{i,u}), \tag{1}$$

where $m = -\ln 2/\ln(\cos\Phi_{1/2})$ denotes the Lambertian emission order, and $\Phi_{1/2}$ is the angle of half intensity; A_{pd} is the physical area of the PD; g_f is the gain of the optical filter; the optical concentrator gain $g_c(\psi_{i,u})$ is given by [17, eq. (8)]:

$$g_c(\psi_{i,u}) = \begin{cases} \dfrac{n^2}{\sin^2(\Psi_{\text{max}})}, & 0 \le \psi_{i,u} \le \Psi_{\text{max}} \\ 0, & \psi_{i,u} > \Psi_{\text{max}} \end{cases}, \tag{2}$$

where n denotes the refractive index, and Ψ_{max} is the semi-angle of the field of view (FoV) of the PD.

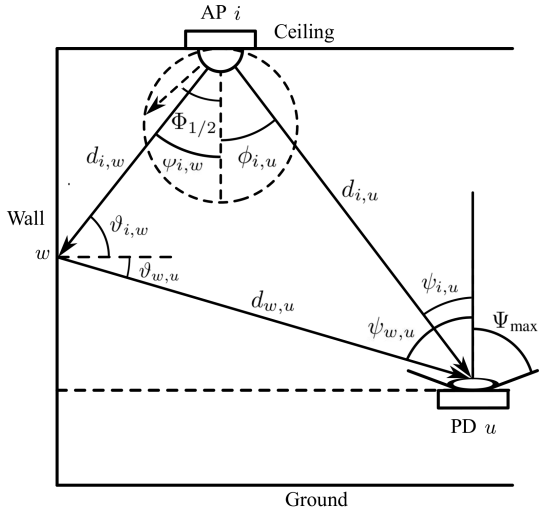

Fig. 1. The LoS and first-order NLoS paths of the LiFi channel [18].

A first-order reflection consists of two segments: i) from the AP to a small area w on the wall, and ii) from w to the user. The Euclidean distances of these two segments are denoted by $d_{i,w}$ and $d_{w,u}$. The angles of radiance and incidence regarding the first segment are $\phi_{i,w}$ and $\vartheta_{i,w}$, and for the second segment they are $\vartheta_{w,u}$ and $\psi_{w,u}$. The channel gain of NLoS is written as follows:

$$H^{i,u}_{\text{NLoS}} = \int_{A_w} \frac{(m+1)A_{\text{pd}}}{2(\pi d_{i,w} d_{w,u})^2} \rho_w \cos^m(\phi_{i,w}) g_f g_c(\psi_{w,u}) \cos(\psi_{w,u}) \cos(\vartheta_{i,w}) \cos(\vartheta_{w,u}) dA_w, \tag{3}$$

where A_w is the area of w and ρ_w denotes the wall reflectivity.

Adding (1) to (3), the total gain of the LiFi channel can be expressed as follows:

$$H_{\text{LiFi}}^{i,u} = H_{\text{LoS}}^{i,u} + H_{\text{NLoS}}^{i,u}. \tag{4}$$

At the receiver, the PD converts the captured photons into an electric current:

$$I_{\text{elec}} = R_{\text{pd}} H_{\text{LiFi}}^{i,u} P_{\text{opt}}/\zeta, \tag{5}$$

where R_{pd} is the detector responsivity; P_{opt} denotes the transmitted optical power; and ζ is the ratio of P_{opt} to the optical signal power. The signal-to-noise ratio (SNR) of the user is denoted by $\gamma^{i,u}$, which can be written as follows:

$$\gamma^{i,u} = \frac{(R_{\text{pd}} H_{\text{LiFi}}^{i,u} P_{\text{opt}}/\zeta)^2}{N_{\text{LiFi}} B_{\text{LiFi}}}, \tag{6}$$

where N_{LiFi} denotes the power spectral density (PSD) of noise at the receiver, including shot noise and thermal noise, while B_{LiFi} is the bandwidth of the LiFi AP.

III. Standard Handover Scheme

In order to tackle the ping-pong effect, the handover scheme in LTE [11] introduces two parameters: handover margin (HOM) and time to trigger (TTT). Fig. 2 shows the principle of this scheme, which is referred to as STD in the remainder of this paper.

The RSRP of the host AP is denoted by P_{i_H}, and the RSRP of the target AP is denoted by P_{i_T}. Let δ_{HOM} denote the value of HOM. The STD scheme starts counting time when the following condition is satisfied:

$$P_{i_T} > P_{i_H} + \delta_{\text{HOM}}. \tag{7}$$

The time counter continues as long as (7) is satisfied, and otherwise is reset. Let t_{TTT} denote the value of TTT. When the time counter reaches t_{TTT}, a handover decision is made to transfer the user from the host AP to the target AP.

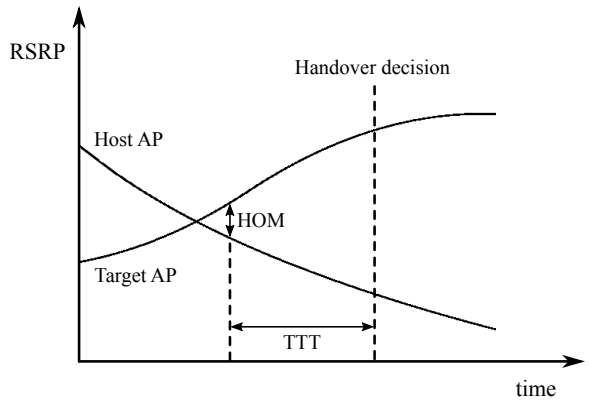

Fig. 2. The handover scheme in LTE.

Fig. 3 exemplifies the movement paths of the user in a LiFi network. The STD scheme can guarantee a minimum connection time equal to t_{TTT}, which is usually limited to hundreds of milliseconds [11]. Thus, this scheme is capable of skipping some APs that the user crosses very quickly, such as Path 1. In this case, the user is directly transferred from AP A to AP C, with AP B being skipped. However, this scheme cannot skip the APs where the user stays longer than t_{TTT}, even slightly. Taking Path 2 for example, STD would handover the user from AP A to AP B, and then from AP B to AP C. Also, it is worth noting that the user might experience random light-path blockages [19]. This can be deemed as an infinite attenuation for the link between the user and the blocked APs. The impact of random light-path blockages on handover rates will be studied in Section VI-E.

IV. Proposed Handover Skipping Method

The value of RSRP reflects the distance between the AP and the user, and a higher RSRP signifies the corresponding AP is closer to the user. For example, when the user crosses the border between AP A and AP B in Fig. 3, AP B offers a higher RSRP than AP C. However, in Path 1 and Path 2, the user passes the outskirts of AP B and moves towards the central area of AP C. As a result, AP C provides a faster increase in RSRP than AP B. With respect to Path 3,

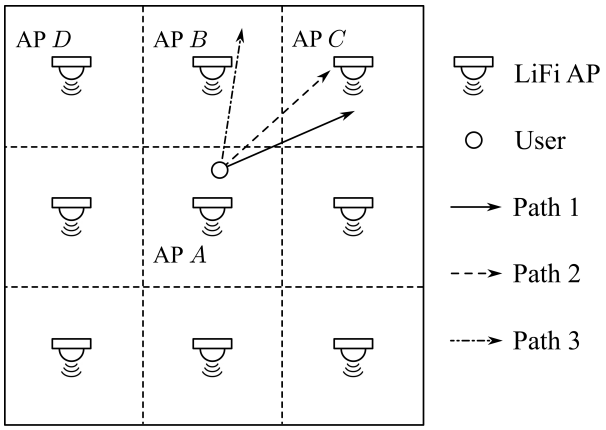

Fig. 3. Different movement paths of the user in a LiFi network.

the user moves towards the central area of AP B and thus gains a rapidly increasing RSRP from AP B. The RSRP and the change in RSRP can be used together to determine whether an AP needs to be skipped. The objective function of the target AP is denoted by Γ_i, and it is formulated as follows:

$$\Gamma_i = P_i^{(t_0)} + \lambda \Delta P_i, \tag{8}$$

where t_0 denotes the starting point of the time counter; $P_i^{(t_0)}$ is the RSRP of AP i at t_0; λ is the weight coefficient and its optimal value will be studied in Section VI-A; and ΔP_i denotes the change in RSRP per time unit, which is expressed as:

$$\Delta P_i = \frac{P_i^{(t_0+t_{\text{TTT}})} - P_i^{(t_0)}}{t_{\text{TTT}}}. \tag{9}$$

With the proposed method, the time counter works in the same way as in STD. When the time counter reaches t_{TTT}, the proposed method would select the AP with the largest Γ_i to be the target AP. Note that the target AP does not have to be the one that triggers the time counter, e.g. AP B in Fig. 3. At the end of the time counter, a handover will be executed immediately if the target AP already meets the condition in (7). Otherwise, the handover will be held on until the target AP meets the condition. During this period, the target AP could be recalculated if the

direction or speed of the user's movement changes. Let $\mathcal{I}$ denote the set of all candidate APs. The output of the time counter is denoted by t_c. The pseudo code of the proposed handover skipping method is given in Algorithm 1.

Algorithm 1 Proposed Handover Skipping Method

Input: $P_H^{(t)}$, $P_i^{(t)}$, $\forall i \in \mathcal{I}$

Output: i_T

$t_c \Leftarrow 0$

while $t_c < t_{\text{TTT}}$ **do**

if $P_i^{(t)} \leq P_H^{(t)} + \delta_{\text{HOM}}, \forall i \in \mathcal{I}$ **then**

$t_c \Leftarrow 0$

else if $t_c = 0$ **then**

$t_0 \Leftarrow t$

else

$t_c \Leftarrow t - t_0$

end if

$t \Leftarrow t + 1$

end while

$\Gamma_i \Leftarrow P_i^{(t_0)} + \lambda \left(P_i^{(t_0+t_{\text{TTT}})} - P_i^{(t_0)} \right) / t_{\text{TTT}}$

$i_T \Leftarrow \max\{\Gamma_i\}$

Note that in (8), $P_i^{(t_0)}$ depends on the position of the point that the user crosses the border, whereas ΔP_i reflects the direction and speed of the user's movement. If the crossing point is very close to the border between two candidate APs, e.g. AP B and AP C in Path 1, the RSRP offered by those APs would be almost the same. In this case, ΔP_i is the dominant factor to determine the target AP. On the contrary, the values of RSRP significantly differ when the crossing point is

far away from one candidate AP, e.g. AP C in Path 3. In this case, $P_i^{(t_0)}$ becomes the dominant factor. As for Path 2, AP B provides an RSRP marginally higher than AP C. Meanwhile, the ΔP_i of AP C increases with the user's speed. If the user moves fast, it is handed over from AP A to AP C, with AP B being skipped. Otherwise, the user is transferred to AP B due to the insignificant influence of ΔP_i.

V. Theoretical Analysis of Handover Skipping Performance

In this section, the theoretical performance of the proposed handover skipping method is analysed for an arbitrary line trajectory. The area covered by the LiFi network is assumed to be boundless. Thus, only LoS paths need to be taken into account.

A. Handover Rate

First, we analyse the handover rate of the SSS method, where there is no handover skip. We focus on the square deployment of LiFi APs as it is commonly used in practice to provide uniform illumination. The handover rate with the Poisson point process (PPP) deployment can be found in [20]. It is assumed that the user enters the coverage area of an AP at an arbitrary point δ with an arbitrary angle θ. Let r denote the length of the side of the coverage area. The length of the user's movement path inside the coverage area is denoted by d_{path}. The average value of d_{path} is denoted by $\bar{d}_{\text{path}}$, which is derived in Appendix A. The handover rate in this case is denoted by η, which is equal to the user's speed v divided by $\bar{d}_{\text{path}}$:

$$\eta = \frac{\pi v}{r}\left[3\log\left(\sqrt{2}+1\right)+1-\sqrt{2}\right]^{-1}. \tag{10}$$

Then we derive the probability of handover skipping. With the proposed method, the user skips an AP when there exists another AP providing a larger Γ_i. This event is denoted by X and its probability $\mathbb{P}(X)$ can be expressed as follows:

$$\mathbb{P}(X) = 1 - \mathbb{P}(\neg X), \tag{11}$$

where:

$$\mathbb{P}(\neg X) = \mathbb{P}(\Gamma_B \geq \Gamma_i, \forall i, i \neq B). \tag{12}$$

With the square deployment, the host AP borders 8 neighbours. Further APs are unlikely to become the handover target due to the much lower RSRP they provide. Let's consider the case that the user leaves AP A and enters AP B, as shown in Fig. 3. AP C and AP D are the only possible candidates for handover skipping, as in comparison with them the remaining neighbours perform worse in terms of both P and ΔP. Since the square deployment is axisymmetric, we assume that the user crosses the right half segment of the border between AP A and AP B. The candidate for handover skipping could only be AP C if θ is less than 90°, and otherwise AP D. Therefore, $\mathbb{P}(\neg X)$ can be rewritten as:

$$\mathbb{P}(\neg X) = \int_{\delta=0}^{r/2} \mathbb{P}(\neg X \mid \delta)\mathbb{P}(\delta)d\delta, \tag{13}$$

where:

$$\mathbb{P}(\neg X \mid \delta) = \int_{\theta=0}^{\pi/2} \mathbb{P}(\Gamma_B \geq \Gamma_C \mid \theta, \delta)\mathbb{P}(\theta)d\theta + \int_{\theta=\pi/2}^{\pi} \mathbb{P}(\Gamma_B \geq \Gamma_D \mid \theta, \delta)\mathbb{P}(\theta)d\theta. \tag{14}$$

See the expressions of $\mathbb{P}(\Gamma_B \geq \Gamma_C \mid \theta, \delta)$ and $\mathbb{P}(\Gamma_B \geq \Gamma_D \mid \theta, \delta)$ in Appendix B. Since θ is uniformly distributed between 0 and π, the above equation can be rewritten as:

$$\mathbb{P}(\neg X \mid \delta) = \frac{\Theta_D(\delta) - \Theta_C(\delta)}{\pi}. \tag{15}$$

As δ is uniformly distributed between 0 and $\frac{r}{2}$, we have $\mathbb{P}(\delta) = \frac{2}{r}$. Therefore, (13) can be computed as follows:

$$\mathbb{P}(\neg X) = \frac{2}{\pi r} \int_{\delta=0}^{r/2} \left[\Theta_D(\delta) - \Theta_C(\delta)\right] d\delta. \tag{16}$$

The handover rate of the proposed method is denoted by η_{HS}, which is the product of η and $\mathbb{P}(\neg X)$. Combining (10) and (16), η_{HS} can be expressed as:

$$\eta_{\text{HS}} = \frac{2v}{r^2} \left[3\log\left(\sqrt{2}+1\right) + 1 - \sqrt{2}\right]^{-1} \int_{\delta=0}^{r/2} \left[\Theta_D(\delta) - \Theta_C(\delta)\right] d\delta. \tag{17}$$

B. Coverage Probability

The coverage probability is defined as the probability that a user's SNR is above a certain threshold γ_T. This threshold corresponds to a certain horizontal distance between the user and the AP, which is denoted by l_T. According to (6), l_T can be computed as follows:

$$l_T = \sqrt{\left[\frac{(m+1)A_{\text{pd}}h^{m+1}g_f g_c R_{\text{pd}} P_{\text{opt}}}{2\pi\zeta\sqrt{\gamma_T N_{\text{LiFi}} B_{\text{LiFi}}}}\right]^{\frac{2}{m+3}} - h^2} \tag{18}$$

The user's SNR is larger than γ_T when $l < l_T$. Therefore, the coverage probability of the SSS method is equal to $\mathbb{P}(l < l_T)$. Assuming the user is randomly located in the square coverage area with an equal probability, $\mathbb{P}(l < l_T)$ can be expressed as:

$$\mathbb{P}(l < l_T) = \begin{cases} \pi\left(\dfrac{l_T}{r}\right)^2, & l_T \le \dfrac{r}{2} \\ 2\sqrt{\left(\dfrac{l_T}{r}\right)^2 - \dfrac{1}{4}} + \left(\dfrac{l_T}{r}\right)^2\left[\pi - 4\arccos\left(\dfrac{r}{2l_T}\right)\right], & \dfrac{r}{2} < l_T < \dfrac{\sqrt{2}r}{2} \\ 1, & l_T \ge \dfrac{\sqrt{2}r}{2} \end{cases}. \tag{19}$$

It can be found that the coverage probability of the SSS method depends on the size of the coverage area, and is thus denoted by $\mathcal{P}(r)$. Regarding the proposed method, its coverage probability is equal to $\mathcal{P}(r)$ when no handover skipping occurs. When there is a handover skip, the distance between the host and target APs changes from r to $\sqrt{2}r$. The coverage probability of the proposed method can be estimated as follows:

$$\mathcal{P}_{\text{HS}}(r) = \mathbb{P}(\neg X)\mathcal{P}(r) + \mathbb{P}(X)\mathcal{P}(\sqrt{2}r). \tag{20}$$

However, the skipped AP is located at one end-point of the border between the host and target APs, making this corner area unlikely to be involved in handover skipping. Therefore, (20) would underestimate the SNR of the user in the lower end. More details will be given in the following section.

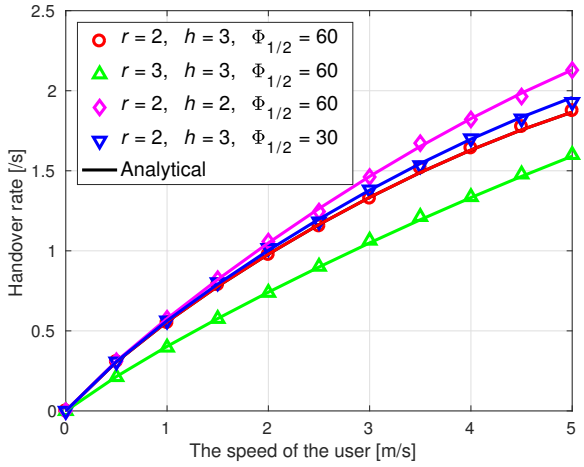

Fig. 4. Handover rate versus the user's speed.

C. Validation

Monte Carol simulations are conducted to verify the above theoretical analysis. Here the weight λ is fixed to be 1. In Fig. 4, the handover rate is shown as a function of the user's speed. As can be seen, the analytical results in (17) closely match the simulations. In addition, the handover rate decreases when: i) the distance between the nearest APs increases; or ii) the vertical distance between the user and the AP increases; or iii) the half-intensity angle of the LED increases.

Taking $v = 5$ m/s as an example, Fig. 5 presents the coverage probability of the proposed method. The impact of the user's speed will be studied in the following section. In general, the estimated expression agrees with the simulations. For lower SNRs, the analytical results are below the simulations with a marginal gap, as explained. Also, it can be found that the noted three situations all result in a decrease in SNR. In summary, the handover rate can be reduced at the cost of a decreasing SNR.

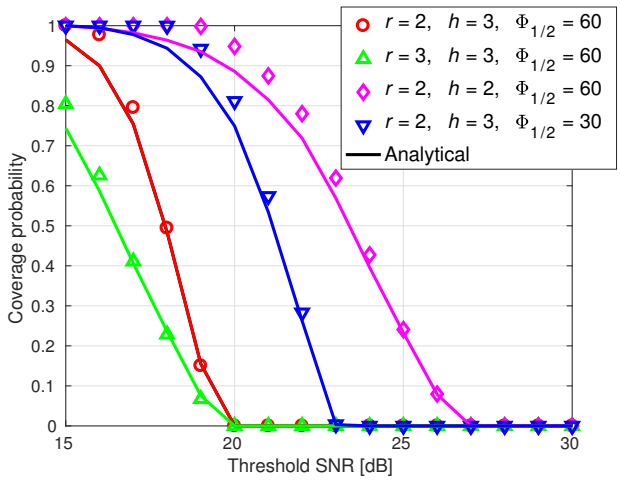

Fig. 5. Coverage probability versus threshold SNR.

VI. Simulation Results

In this section, Monte Carlo simulations are conducted to evaluate the performance of the proposed method. The STD and trajectory-based handover skipping methods are considered as benchmarks. In order to provide a fair comparison, the same HOM and TTT are used in the three methods. Here the values of HOM and TTT are set to be 1 dB and 160 ms [11]. In addition, we consider 16 LiFi APs and the separation between the two nearest APs is fixed to be 2m. Other required parameters are summarised in Table I.

A. The Impact of the Weight Coefficient

First, we study the effect of λ on the performance of the proposed method. Note that λ needs to be larger than t_{TTT}, as stated in Lemma A.2. Different speeds of the user in four movement scenarios are considered: 0.1 m/s (slowly moving), 1.4 m/s (walking), 5 m/s (running) and 10 m/s (sprinting). As shown in Fig. 6, for a slowly moving user, the throughput almost remains the same as λ varies in the displayed range. This is because in this case, the change of RSRP is very insignificant in determining the handover target. As the speed increases to 1.4 m/s, choosing a

TABLE I

SIMULATION PARAMETERS

Parameter	**Value**
Room size (length by width by height)	8m $\times$ 8m $\times$ 3m
The physical area of a PD, A_{pd}	1 cm^2
The gain of the optical filter, g_f	1
The refractive index, n	1.5
Half-intensity radiation angle, $\Phi_{1/2}$	60°
FoV semi-angle of PD, Ψ_{max}	90°
Transmitted optical power, P_{opt}	3 Watt
The ratio of P_{opt} to the optical signal power, ζ	3
Detector responsivity, R_{pd}	0.53 A/W
Wall reflectivity, ρ_w	0.8
Bandwidth per LiFi AP, B_{LiFi}	200 MHz
PSD of noise in LiFi, N_{LiFi}	10^{-21} A^2/Hz
Handover overhead	200 ms [21]

proper λ becomes crucial. On the one hand, a too small λ would disable the function of handover skipping. On the other hand, a too large λ would cause unnecessary handover skipping. For a fast moving user, the throughput is a monotonically increasing function of λ in the displayed range. The reason is that the change of RSRP becomes a dominant factor in this case. Considering the optimal solutions to different speeds of the user, λ is set to be 1 in the following simulations.

B. Handover Rate

Second, the handover rate performance of the proposed method is studied. Fig. 7 presents the decreases in handover rate provided by the proposed method against STD and the trajectory-based method. The following outcomes are observed: i) compared to the baseline methods, the

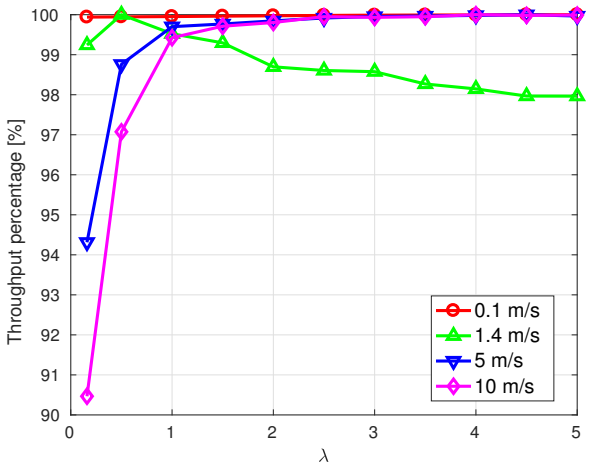

Fig. 6. Throughput versus the weight coefficient for different speeds of the user.

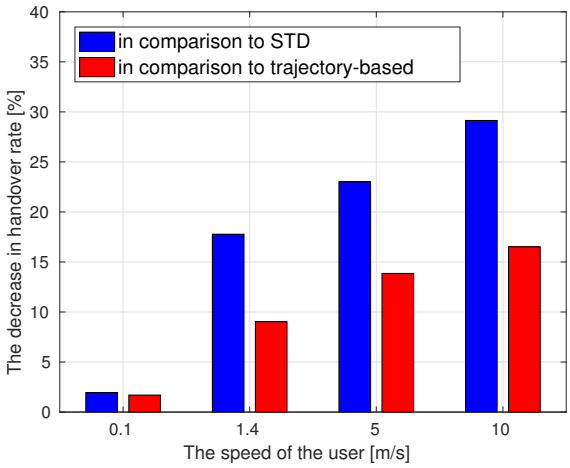

Fig. 7. The decrease in handover rate versus the speed of the user.

proposed method can effectively decrease the handover rate for different speeds of the user; and ii) as the speed of the user increases, this decrease in handover rate becomes larger. At $v = 0.1$ m/s, the proposed method achieves a handover rate 2% less than STD. When v increases to 1.4 m/s, this gap increases to 18%. For $v = 10$ m/s, the proposed method reduces the handover rate over STD by 29%, and compared to the trajectory-based method this gap is 17%.

C. Coverage Probability

Third, the coverage probability for different speeds of the user in shown in Fig. 8. Here the SSS method is considered as a baseline, because its host AP only depends on the user's location, regardless of the user's speed. This method can be deemed as a special case of STD with zero HOM and TTT. As shown, the coverage probability of the proposed method decreases as the user's speed increases, especially for medium SNRs between 14 and 18 dB. High SNRs correspond to the cell centre, where the handover skipping rarely occurs; low SNRs correspond to the cell corner, where the target AP of handover skipping can provide a comparable SNR against the skipped AP. Otherwise, the SNR performance would substantially decrease when the handover skipping happens. Nevertheless, for the 50-th percentile, the SNR of the proposed method is only 2 dB less than that of SSS at most. This means that with the proposed method, the user can achieve an SNR comparable to that of SSS in at least 50% of situations. Also, it is observed that at $v = 10$ m/s, there is a noticeable gap between the coverage probabilities of the proposed method and the trajectory-based method at lower SNRs. This is because when the user moves very fast, the proposed method might skip more than one AP, leading to a significant decrease in SNR.

D. Throughput

In Fig. 9, the user's throughput is presented as a function of the user's speed. The throughput is mearsured by the modulation and coding scheme in [22], and no data transmission is counted during the process of handover. As shown, the proposed method always achieves a higher throughput than the baseline methods. This gain becomes more significant as the user's speed increases. For $v = 5$ m/s, the proposed method can improve the throughput over STD and the trajectory-based method by 17% and 5%. When v increases to 10 m/s, the corresponding values increase to 66% and 26%, respectively.

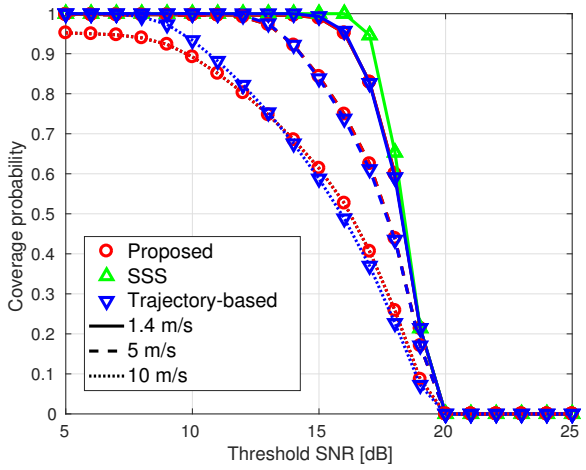

Fig. 8. Coverage probability for different speeds of the user.

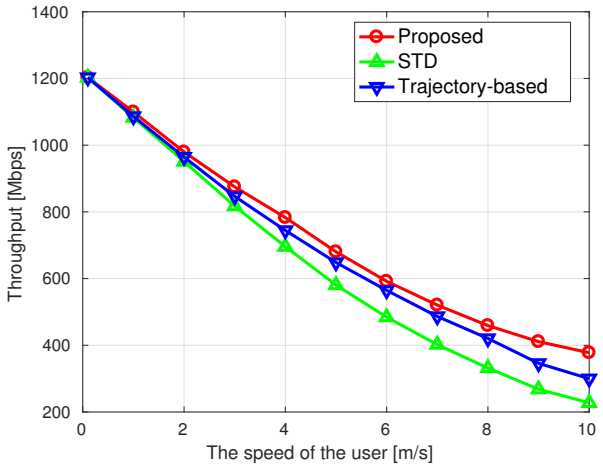

Fig. 9. Throughput versus the speed of the user.

E. The Impact of Random Light-path Blockages

Finally, we study the impact of random light-path blockages on handover rates. In queueing theory [23], the Poisson point process is widely used to model random events such as the arrival of packages at a switch. Here the events of light-path blockages are also assumed to follow the Poisson distribution, and its mean is referred to as the occurrence rate. As shown in Fig. 10,

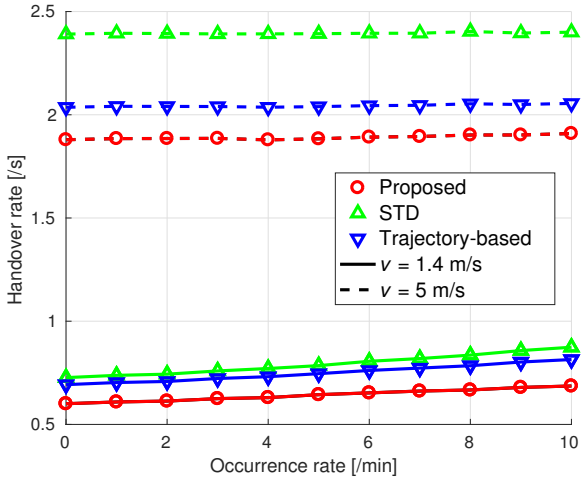

Fig. 10. Handover rate versus the occurrence rate.

the handover rates of all involved methods noticeably increase with the occurrence rate in the case of $v = 1.4$ m/s. While the user's speed increases to 5 m/s, the corresponding handover rate is hardly affected by the change in occurrence rate. This is because for the user moving at a relatively high speed, in comparison to user mobility, the random light-path blockage is an insignificant factor that affects the handover process.

VII. Conclusion

In this paper, a novel handover skipping method was proposed for LiFi networks. Unlike the conventional methods using the user's trajectory information, the proposed method is based on RSRP, which has been commonly used in the current handover schemes. Therefore, the proposed method does not require additional feedback and can be readily implemented in practice. Specifically, the change of RSRP is exploited to reflect whether a user is moving towards the AP. The weighted average of this parameter and the value of RSRP is used to determine the target AP for handover. Also, the handover rate and coverage probability of the proposed method is theoretically analysed. Furthermore, the effect of the weight coefficient on

the performance of the proposed method is studied. Simulation results show that the proposed method can significantly reduce the handover rate against STD, especially when the user is moving relatively fast. Regarding the system throughput, the proposed method outperforms STD and the trajectory-based handover skipping method by up to 66% and 26%, respectively. Future research will study the issue of handover skipping in hybrid LiFi and WiFi networks.

ACKNOWLEDGEMENT

This work was supported by the Engineering and Physical Sciences Research Council (EPSRC) grant EP/L020009/1: Towards Ultimate Convergence of All Networks (TOUCAN). Professor Harald Haas greatly acknowledges support from the EPSRC under Established Career Fellowship Grant EP/K008757/1.

REFERENCES

[1] X. Wu and H. Haas, "RSRP-based handover skipping for ultra-dense networks," in *IEEE 89th Vehicular Technology Conf. (VTC Spring)*, Kuala Lumpur, Apr. 2019, pp. 1–5.

[2] "Cisco visual networking index: Forecast and trends, 2017-2022," Cisco, Tech. Rep., Nov. 2018.

[3] T. S. Rappaport, S. Sun, R. Mayzus, H. Zhao, Y. Azar, K. Wang, G. N. Wong, J. K. Schulz, M. Samimi, and F. Gutierrez, "Millimeter wave mobile communications for 5G cellular: It will work!" *IEEE Access*, vol. 1, pp. 335–349, 2013.

[4] H. Q. Ngo, A. Ashikhmin, H. Yang, E. G. Larsson, and T. L. Marzetta, "Cell-free massive MIMO versus small cells," *IEEE Trans. Wireless Commun.*, vol. 16, no. 3, pp. 1834–1850, Mar. 2017.

[5] H. Burchardt, N. Serafimovski, D. Tsonev, S. Videv, and H. Haas, "VLC: Beyond point-to-point communication," *IEEE Commun. Mag.*, vol. 52, no. 7, pp. 98–105, July 2014.

[6] H. Haas, L. Yin, Y. Wang, and C. Chen, "What is LiFi?" *Journal of Lightwave Technol.*, vol. 34, no. 6, pp. 1533–1544, March 2016.

[7] M. Islim *et al.*, "Towards 10 Gb/s orthogonal frequency division multiplexing-based visible light communication using a GaN violet microLED," *Photon. Res.*, vol. 5, no. 2, pp. A35–A43, Apr. 2017.

[8] L. Hanzo, H. Haas, S. Imre, D. O'Brien, M. Rupp, and L. Gyongyosi, "Wireless myths, realities, and futures: From 3G/4G to optical and quantum wireless," *Proceedings of the IEEE*, vol. 100, no. Special Centennial Issue, pp. 1853–1888, May 2012.

[9] H. Haas, "Visible light communication," in *2015 Optical Fiber Communications Conf. and Exhibition (OFC)*, Los Angeles, CA, Mar. 2015, pp. 1–72.

[10] I. Stefan, H. Burchardt, and H. Haas, "Area spectral efficiency performance comparison between VLC and RF femtocell networks," in *2013 IEEE Int. Conf. on Communications (ICC)*, Jun. 2013, pp. 3825–3829.

[11] 3GPP TS 36.331 v12.7.0., "EUTRA radio resource control (Release 12)," Sep. 2015.

[12] R. Arshad, H. Elsawy, S. Sorour, T. Y. Al-Naffouri, and M. Alouini, "Handover management in 5G and beyond: A topology aware skipping approach," *IEEE Access*, vol. 4, pp. 9073–9081, 2016.

[13] E. Demarchou, C. Psomas, and I. Krikidis, "Mobility management in ultra-dense networks: Handover skipping techniques," *IEEE Access*, vol. 6, pp. 11 921–11 930, 2018.

[14] R. Arshad, H. ElSawy, S. Sorour, T. Y. Al-Naffouri, and M. Alouini, "Velocity-aware handover management in two-tier cellular networks," *IEEE Trans. Wireless Commun.*, vol. 16, no. 3, pp. 1851–1867, Mar. 2017.

[15] A. A. Purwita, M. D. Soltani, M. Safari, and H. Haas, "Impact of terminal orientation on performance in LiFi systems," in *2018 IEEE Wireless Communications and Networking Conf. (WCNC)*, Barcelona, Apr. 2018, pp. 1–6.

[16] D. Johnson and D. Maltz, "Dynamic source routing in ad hoc wireless networks," *Mobile Computing*, pp. 153–181, 1996.

[17] J. Kahn and J. Barry, "Wireless infrared communications," *IEEE Proceedings*, vol. 85, no. 2, pp. 265–298, Feb. 1997.

[18] X. Wu, M. Safari, and H. Haas, "Access point selection for hybrid Li-Fi and Wi-Fi networks," *IEEE Trans. Commun.*, vol. 65, no. 12, pp. 5375–5385, Dec. 2017.

[19] X. Wu and H. Haas, "Access point assignment in hybrid LiFi and WiFi networks in consideration of LiFi channel blockage," in *IEEE 18th Int. Workshop on Signal Processing Advances in Wireless Communications (SPAWC)*, Sapporo, July 2017, pp. 1–5.

[20] W. Bao and B. Liang, "Stochastic geometric analysis of handoffs in user-centric cooperative wireless networks," in *IEEE 35th Annual Int. Conf. on Computer Communications (INFOCOM)*, San Francisco, CA, Apr. 2016, pp. 1–9.

[21] J. Xiao and F. Liu, "A pre-scanning fast handoff scheme for VoIP in WLANs," *International Journal of Future Computer and Communication*, vol. 8, no. 2, pp. 343–354, 2015.

[22] "Ieee standard for information technology– local and metropolitan area networks– specific requirements– part 11: Wireless lan medium access control (mac)and physical layer (phy) specifications amendment 5: Enhancements for higher throughput," *IEEE Std 802.11n-2009 (Amendment to IEEE Std 802.11-2007 as amended by IEEE Std 802.11k-2008, IEEE Std 802.11r-2008, IEEE Std 802.11y-2008, and IEEE Std 802.11w-2009)*, pp. 1–565, Oct. 2009.

[23] L. Kleinrock, *Queueing Systems: Theory*. West Sussex, U.K.: Wiley, 1976.

APPENDIX

A. Derivation of $\bar{d}_{path}$

For a certain entry point, there are four types of possible paths, as shown in Fig. 11. Each type corresponds to a mathematical expression of $d_{\text{path}}(\delta)$:

$$d_{\text{path}}(\delta) = \begin{cases} \dfrac{\delta}{\cos(\theta)}, & 0 \le \theta < \theta_1 \\ \dfrac{r}{\sin(\theta)}, & \theta_1 \le \theta < \dfrac{\pi}{2} \\ \dfrac{r}{\sin(\pi-\theta)}, & \dfrac{\pi}{2} \le \theta < \theta_2 \\ \dfrac{r-\delta}{\cos(\pi-\theta)}, & \theta_2 \le \theta \le \pi \end{cases}, \tag{21}$$

where:

$$\begin{cases} \theta_1 = \arctan\left(\dfrac{r}{\delta}\right) \\ \theta_2 = \pi - \arctan\left(\dfrac{r}{r-\delta}\right) \end{cases}. \tag{22}$$

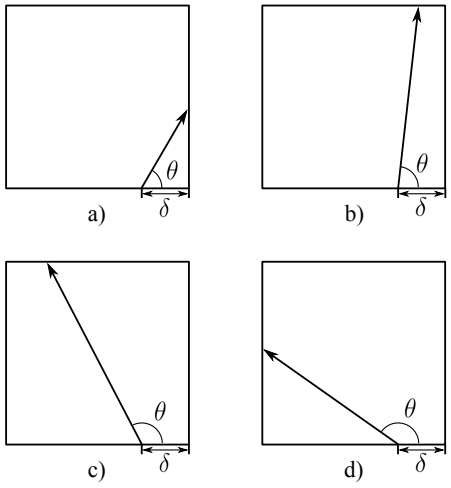

Fig. 11. The movement paths of the user in the coverage area of an AP.

Since $\sin(\pi-\theta)=\sin(\theta)$, the second and third types can be merged into one. The average value of $d_{\text{path}}(\delta)$ can be calculated as follows:

$$\bar{d}_{\text{path}}(\delta)=\frac{1}{\pi}\left(\int_{\theta=0}^{\theta_1}\frac{\delta}{\cos(\theta)}d\theta+\int_{\theta=\theta_1}^{\theta_2}\frac{r}{\sin(\theta)}d\theta+\int_{\theta=\theta_2}^{\pi}\frac{\delta-r}{\cos(\theta)}d\theta\right). \tag{23}$$

The integrals on the right side of the above equation can be solved by calculating the antiderivatives. Consequently, the above equation can be expressed as follows:

$$\bar{d}_{\text{path}}(\delta)=\frac{1}{\pi}\left[\delta\log\left(\frac{r+\delta_1}{\delta}\right)+r\log\left(\frac{\delta+\delta_1}{\delta_2-r+\delta}\right)+(r-\delta)\log\left(\frac{r+\delta_2}{r-\delta}\right)\right]. \tag{24}$$

where:

$$\begin{cases}\delta_1=\sqrt{\delta^2+r^2}\\ \\ \delta_2=\sqrt{(r-\delta)^2+r^2}\end{cases}. \tag{25}$$

With δ varying from 0 to $\dfrac{r}{2}$, the parameter $\bar{d}_{\text{path}}$ is computed by:

$$\bar{d}_{\text{path}}=\frac{2}{r}\int_{\delta=0}^{\frac{r}{2}}\bar{d}_{\text{path}}(\delta)d\delta. \tag{26}$$

Substituting (24) into (26), $\bar{d}_{\text{path}}$ can be expressed as follows:

$$\bar{d}_{\text{path}}=\frac{r}{\pi}\left[3\log\left(\sqrt{2}+1\right)+1-\sqrt{2}\right]. \tag{27}$$

B. Derivation of $\mathbb{P}(\Gamma_B\geq\Gamma_C\mid\theta,\delta)$ *and* $\mathbb{P}(\Gamma_B\geq\Gamma_D\mid\theta,\delta)$

According to (1), (5) and (8), Γ_i can be written as follows:

$$\Gamma_i=g_{\text{eff}}\left[\left(1-\frac{\lambda}{t_{\text{TTT}}}\right)\mathcal{P}_i^{(t_0)}+\frac{\lambda}{t_{\text{TTT}}}\mathcal{P}_i^{(t_0+t_{\text{TTT}})}\right], \tag{28}$$

where:

$$g_{\text{eff}}=\left[\frac{(m+1)A_{\text{pd}}g_f g_c R_{\text{pd}}P_{\text{opt}}}{2\pi\zeta}\right]^2\left(h_{i,u}^{(t)}\right)^{2m+2}, \tag{29}$$

and:

$$\mathcal{P}_i^{(t)}=\left[\left(h_{i,u}^{(t)}\right)^2+\left(l_{i,u}^{(t)}\right)^2\right]^{-m-3}, \tag{30}$$

where $h_{i,u}^{(t)}$ and $l_{i,u}^{(t)}$ denote the vertical and horizontal distances between AP i and user u, respectively. Since all APs are assumed to lie on the same level, $h_{i,u}^{(t)}$ is a constant and thus can be abbreviated to h.

Removing the common items in Γ_B and Γ_C, $\mathbb{P}(\Gamma_B \geq \Gamma_C \mid \theta, \delta)$ can be rewritten as:

$$\mathbb{P}(\Gamma_B \geq \Gamma_C \mid \theta, \delta) = \mathbb{P}(Z(\theta) \geq 0 \mid \theta, \delta), \tag{31}$$

where:

$$Z(\theta) = \left(1 - \frac{\lambda}{t_{\text{TTT}}}\right)\left(\mathcal{P}_B^{(t_0)} - \mathcal{P}_C^{(t_0)}\right) + \frac{\lambda}{t_{\text{TTT}}}\left(\mathcal{P}_B^{(t_0+t_{\text{TTT}})} - \mathcal{P}_C^{(t_0+t_{\text{TTT}})}\right). \tag{32}$$

Given δ and θ, we have:

$$\begin{cases} l_{B,u}^{(t_0)} = \sqrt{\left(\frac{r}{2}\right)^2 + \left(\frac{r}{2} - \delta\right)^2} \\ l_{B,u}^{(t_0+t_{\text{TTT}})} = \sqrt{\left(\frac{r}{2} - vt_{\text{TTT}}\sin(\theta)\right)^2 + \left(\frac{r}{2} - \delta + vt_{\text{TTT}}\cos(\theta)\right)^2} \\ l_{C,u}^{(t_0)} = \sqrt{\left(\frac{r}{2}\right)^2 + \left(\frac{r}{2} + \delta\right)^2} \\ l_{C,u}^{(t_0+t_{\text{TTT}})} = \sqrt{\left(\frac{r}{2} - vt_{\text{TTT}}\sin(\theta)\right)^2 + \left(\frac{r}{2} + \delta - vt_{\text{TTT}}\cos(\theta)\right)^2} \end{cases}. \tag{33}$$

Lemma A.1: For $\theta \in \left[0, \frac{\pi}{2}\right]$, $Z(\theta)$ is monotonically decreasing up to some point and then monotonically increasing if $\mathcal{P}_B^{(t_0+t_{\text{TTT}})} - \mathcal{P}_C^{(t_0+t_{\text{TTT}})} < 0$, and otherwise monotonically increasing.

Proof: Note that the item $\left(1 - \frac{\lambda}{t_{\text{TTT}}}\right)\left(\mathcal{P}_B^{(t_0)} - \mathcal{P}_C^{(t_0)}\right)$ in (32) is a constant with respect to θ. Therefore, $Z(\theta)$ changes along with $\left(\mathcal{P}_B^{(t_0+t_{\text{TTT}})} - \mathcal{P}_C^{(t_0+t_{\text{TTT}})}\right)$, which is denoted by $F(\theta)$. Let $F_1(\theta)$ and $F_2(\theta)$ denote $\left(l_{B,u}^{(t_0+t_{\text{TTT}})}\right)^2$ and $\left(l_{C,u}^{(t_0+t_{\text{TTT}})}\right)^2$, respectively. The derivative of $F_1(\theta)$ and $F_2(\theta)$ are computed as follows:

$$\begin{cases} F_1'(\theta) = vt_{\text{TTT}}\left[(2\delta - r)\sin(\theta) - r\cos(\theta)\right] \\ F_2'(\theta) = vt_{\text{TTT}}\left[(2\delta + r)\sin(\theta) - r\cos(\theta)\right] \end{cases}. \tag{34}$$

For $\delta \in \left(0, \frac{r}{2}\right)$, we have $2\delta - r < 0$. In addition, since $\theta \in \left[0, \frac{\pi}{2}\right]$, $\sin(\theta)$ and $\cos(\theta)$ are non-negative and cannot be zeros at the same time. Thus $F_1'(\theta)$ is always negative. Note that

$m > 0$ for all possible $\Phi_{1/2}$. Hence, $\mathcal{P}_B^{(t_0+t_{\text{TTT}})}$ is monotonically increasing. As for $F_2'(\theta)$, its derivative $F_2''(\theta)$ is expressed as follows:

$$F_2''(\theta) = vt_{\text{TTT}}\left[(2\delta + r)\cos(\theta) + r\sin(\theta)\right]. \tag{35}$$

Note that $F_2''(\theta)$ is always positive. Also, we have $F_2'(0) = -vt_{\text{TTT}}r < 0$ and $F_2'(\frac{\pi}{2}) = vt_{\text{TTT}}(2\delta + r) > 0$. Therefore there exists one and only one θ meeting $F_2'(\theta) = 0$. This signifies that $\mathcal{P}_C^{(t_0+t_{\text{TTT}})}$ is monotonically increasing until $F_2'(\theta) = 0$ and then monotonically decreasing. It is worth noting that $F_2'(\theta)$ is always larger than $F_1'(\theta)$. This means that when $\mathcal{P}_B^{(t_0+t_{\text{TTT}})}$ and $\mathcal{P}_C^{(t_0+t_{\text{TTT}})}$ are both increasing, $\mathcal{P}_B^{(t_0+t_{\text{TTT}})}$ has a larger slope than $\mathcal{P}_C^{(t_0+t_{\text{TTT}})}$. As a result, $F(\theta)$ is monotonically increasing if $F(0) \geq 0$. Otherwise, $F(\theta)$ is monotonically decreasing first and then monotonically increasing. ■

Lemma A.2: For $\theta \in \left[0, \frac{\pi}{2}\right]$, there is up to one solution to $Z(\theta) = 0$ on condition that $\lambda > t_{\text{TTT}}$.

Proof: According to Lemma A.1, $Z(\theta)$ is monotonically increasing when $F(0) \geq 0$. It is evident that Lemma A.2 is true in this case. When $F(0) < 0$, $Z(\theta)$ is monotonically decreasing first and then monotonically increasing. In this case, Lemma A.2 is true if $Z(0) < 0$. Substituting $\theta = 0$ into (32), we have:

$$Z(0) = \left(1 - \frac{\lambda}{t_{\text{TTT}}}\right)\left(\mathcal{P}_B^{(t_0)} - \mathcal{P}_C^{(t_0)}\right) + \frac{\lambda}{t_{\text{TTT}}}F(0). \tag{36}$$

Note that $\mathcal{P}_B^{(t_0)} - \mathcal{P}_C^{(t_0)}$ is always non-negative and $\dfrac{\lambda}{t_{\text{TTT}}}$ is assumed to be larger than 1. Hence $Z(0) < 0$ when $F(0) < 0$. ■

The coefficient t_{TTT} is very small in practice, with a typical value of 0.16 s [11]. Therefore, the condition $\lambda > t_{\text{TTT}}$ can be readily satisfied. This is also a guideline for the choice of λ.

Lemma A.3: There exists at least one θ to meet $Z(\theta) \geq 0$.

Proof: Substituting $\theta = \dfrac{\pi}{2}$ into (32), we have:

$$Z\left(\tfrac{\pi}{2}\right) = \left(1 - \frac{\lambda}{t_{\text{TTT}}}\right)\left(\mathcal{P}_B^{(t_0)} - \mathcal{P}_C^{(t_0)}\right) + \frac{\lambda}{t_{\text{TTT}}}F\left(\tfrac{\pi}{2}\right). \tag{37}$$

The derivative of $Z\left(\frac{\pi}{2}\right)$ with respect to l is written as:

$$\frac{dZ\left(\frac{\pi}{2}\right)}{dl} = 2(m+3)\left[F_A + F_B + \frac{\lambda}{t_{\text{TTT}}}\left(F_C + F_D - F_A - F_B\right)\right], \tag{38}$$

where:

$$\begin{cases} F_A = \left(\frac{r}{2}+\delta\right)\left[h^2 + \left(\frac{r}{2}\right)^2 + \left(\frac{r}{2}+\delta\right)^2\right]^{-m-4} \\ F_B = \left(\frac{r}{2}-\delta\right)\left[h^2 + \left(\frac{r}{2}\right)^2 + \left(\frac{r}{2}-\delta\right)^2\right]^{-m-4} \\ F_C = \left(\frac{r}{2}+\delta\right)\left[h^2 + \left(\frac{r}{2}-vt_{\text{TTT}}\right)^2 + \left(\frac{r}{2}+\delta\right)^2\right]^{-m-4} \\ F_D = \left(\frac{r}{2}-\delta\right)\left[h^2 + \left(\frac{r}{2}-vt_{\text{TTT}}\right)^2 + \left(\frac{r}{2}-\delta\right)^2\right]^{-m-4} \end{cases}. \tag{39}$$

As mentioned, the coefficient t_{TTT} is very small. In practice, we have $0 \leq vt_{\text{TTT}} < r$ and thus $\left(\frac{r}{2}\right)^2 \geq \left(\frac{r}{2} - vt_{\text{TTT}}\right)^2$. Hence, $F_C \geq F_A$ and $F_D \geq F_B$, leading to $F_C + F_D - F_A - F_B \geq 0$. Also, it is evident that $F_A + F_B > 0$. Thus the derivative of $Z\left(\frac{\pi}{2}\right)$ with respect to δ is always positive. In other words, $Z\left(\frac{\pi}{2}\right)$ is monotonically increasing with δ. Meanwhile, we have $Z\left(\frac{\pi}{2}\right) = 0$ when $\delta = 0$. Therefore, $Z\left(\frac{\pi}{2}\right)$ must be non-negative. ■

Combining the three above lemmas, there is one and only one θ to satisfy $Z(\theta) = 0$ when $F(0) < 0$. For $F(0) \geq 0$, $Z(\theta)$ would be always positive if there does not exist a solution to $Z(\theta) = 0$. Unfortunately, due to the high order of the polynomial in (32), it is difficult to derive a closed-form solution to $Z(\theta) = 0$. Let Θ_C denote this solution if there exists one and otherwise $\Theta_C = 0$. Then $\mathbb{P}(\Gamma_B \geq \Gamma_C \mid \theta, \delta)$ can be computed as follows:

$$\mathbb{P}(\Gamma_B \geq \Gamma_C \mid \theta, \delta) = \begin{cases} 0, & 0 \leq \theta < \Theta_C \\ 1, & \Theta_C \leq \theta \leq \frac{\pi}{2} \end{cases}. \tag{40}$$

Similarly, $\mathbb{P}(\Gamma_B \geq \Gamma_D \mid \theta, \delta)$ can be expressed as follows:

$$\mathbb{P}(\Gamma_B \geq \Gamma_D \mid \theta, \delta) = \begin{cases} 1, & \frac{\pi}{2} < \theta \leq \Theta_D \\ 0, & \Theta_D < \theta \leq \pi \end{cases}, \tag{41}$$

where Θ_D is the solution to $\Gamma_B = \Gamma_D$ if there exists one, and otherwise $\Theta_D = \pi$.